

# Dispersive Excitations in the High-Temperature Superconductor $\text{La}_{2-x}\text{Sr}_x\text{CuO}_4$

N.B. Christensen,<sup>1</sup> D.F. McMorrow,<sup>1,2</sup> H.M. Rønnow,<sup>3,4</sup> B. Lake,<sup>5</sup> S.M. Hayden,<sup>6</sup>  
G. Aeppli,<sup>2</sup> T.G. Perring,<sup>7</sup> M. Mangorntong,<sup>8</sup> M. Nohara,<sup>8</sup> and H. Takagi<sup>8</sup>

<sup>1</sup>*Materials Research Department, Risø National Laboratory, Denmark*

<sup>2</sup>*London Centre for Nanotechnology and Department of Physics and Astronomy, University College London, London, UK*

<sup>3</sup>*ETH-Zürich & Paul Scherrer Institut, Switzerland*

<sup>4</sup>*James Franck Institute, University of Chicago, USA*

<sup>5</sup>*Clarendon Laboratory, University of Oxford, UK*

<sup>6</sup>*H.H. Wills Physics Laboratory, University of Bristol, UK*

<sup>7</sup>*ISIS Facility, Rutherford Appleton Laboratory, UK*

<sup>8</sup>*Institute of Solid State Physics, University of Tokyo, Japan*

High-resolution neutron scattering experiments on optimally doped  $\text{La}_{2-x}\text{Sr}_x\text{CuO}_4$  ( $x=0.16$ ) reveal that the magnetic excitations are dispersive. The dispersion is the same as in  $\text{YBa}_2\text{Cu}_3\text{O}_{6.85}$ , and is quantitatively related to that observed with charge sensitive probes. The associated velocity in  $\text{La}_{2-x}\text{Sr}_x\text{CuO}_4$  appears to be weakly dependent on doping with a value close to the spin wave velocity of the insulating ( $x=0$ ) parent compound. In contrast to the insulator, the excitations broaden rapidly with increasing energy, forming a continuum at higher energy, and bear a remarkable resemblance to multi-particle excitations observed in 1D  $S=1/2$  antiferromagnets. The magnetic correlations are 2D, and so rule out the simplest scenarios where the copper oxide planes are subdivided into weakly interacting 1D magnets.

PACS numbers: PACS numbers: 74.72.Dn, 61.12.-q, 74.25.Ha

The defining properties of any particle or wave-like excitation are the dimensionality of the space in which it moves and its dispersion. Conventional magnets host spin waves, which are coherently precessing deviations of the spins from their equilibrium, ordered configuration. The antiferromagnetic (AF), insulating parents of the high-temperature,  $\text{CuO}_2$  based superconductors are no exception to this rule [1]. An important question is what happens to the magnetic excitations upon chemical doping to produce metals and superconductors. Here we describe experiments on  $\text{La}_{2-x}\text{Sr}_x\text{CuO}_4$  (LSCO), which reveal that the magnetic excitations are in fact dispersive and appear, at least at low energies, to be two-dimensional (2D). However, they are not derived from propagating excitations in the manner of ordinary spin waves. We show how these dispersive spin excitations bear a quantitative relation to those in the  $\text{YBa}_2\text{Cu}_3\text{O}_{6+x}$  (YBCO) family [2, 3], and more astonishingly, to charge sensitive measures of electronic excitations [4, 5]. This discovery clearly establishes the notion of universality amongst the different cuprate families, and will greatly simplify the theory for this highly varied class of complex materials.

The technique chosen is inelastic neutron scattering, which measures the spin excitation spectrum,  $\chi''(\mathbf{Q}, \omega)$ , as a function of both momentum  $\hbar\mathbf{Q}$  and energy  $\hbar\omega$ . Many neutron experiments have been performed on the superconducting (SC) cuprates, and it is fair to ask why another is needed. The reason is that the new MAPS spectrometer at ISIS, UK finally can provide the long sought for definitive results by offering global momentum and energy surveys with momentum resolution as small as  $0.02 \text{ \AA}^{-1}$  rather than the more typical  $0.1 \text{ \AA}^{-1}$ .

Nine single crystals of  $\text{La}_{1.84}\text{Sr}_{0.16}\text{CuO}_4$  (total mass of 18.7 g,  $T_c = 38.5 \text{ K}$ ) grown by the floating zone method were co-aligned with a resulting mosaic spread of  $1.5^\circ$ . The sample was mounted with the SC planes perpendicular to the beam of neutrons with incident energy of 55 meV. Data were collected at 10 and 40 K, and were converted to  $\chi''(\mathbf{Q}, \omega)$  in absolute units of  $\mu_B^2 \text{ eV}^{-1}$  per formula unit (f.u.).

The undoped parent  $\text{La}_2\text{CuO}_4$  displays commensurate AF order giving diffraction at  $\mathbf{Q} = (\pi, \pi)$  (Fig. 1(a)). Upon doping, the diffraction peak splits into four incommensurate (IC) spots [6, 7] reflecting the fact that in real space the AF correlations have become modulated with a period inversely related to  $\delta\pi$ , the distance in reciprocal space from  $(\pi, \pi)$ . In one very popular model [8, 9, 10], the modulation is due to a tendency of the  $\text{CuO}_2$  planes to break into stripes containing 1D magnets. If these magnets were truly independent of each other, they would give rise to perpendicular streaks of scattering. Since there are two equivalent (orthogonal) directions to choose from, a typical sample would produce orthogonal streaks passing through  $(\pi, \pi)$  (Fig. 1(b)). Only an internal modulation along each stripe, as occurs for spin 1/2 chains doped with holes or in an external magnetic field [11], can produce IC features in the neutron scattering images, such as the crossing of streaks from diagonal stripes as depicted in Fig. 1(c).

Figure 1(d)-(f) displays images of  $\chi''(\mathbf{Q}, \omega)$  for  $\text{La}_{1.84}\text{Sr}_{0.16}\text{CuO}_4$ , produced directly from the raw data without performing any background subtraction. They are the first to afford complete (high) isotropic resolution coverage of reciprocal space and energy for superconducting LSCO, and directly reveal a very important

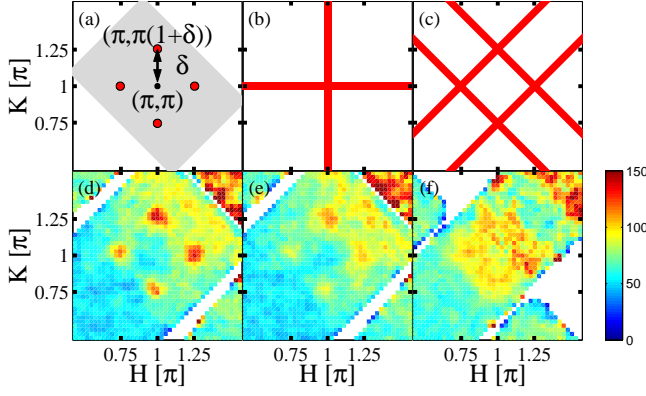


FIG. 1: (a)-(c) 2D reciprocal space indicating the diffraction patterns for different scenarios of the magnetic correlations. (d)-(f) Images from the MAPS spectrometer of the dynamical magnetic susceptibility  $\chi''(\mathbf{Q}, \omega)$  for LSCO  $x = 0.16$ . Colour scale: intensity in units of  $\mu_B^2 \text{ eV}^{-1} \text{ f.u.}^{-1}$ . (d) and (f),  $T = 10 \text{ K}$  in the SC phase for  $\hbar\omega = 10$  and  $30 \text{ meV}$  respectively. (e)  $T = 40 \text{ K}$  in the normal phase at  $10 \text{ meV}$ .

fact. In the SC phase at  $T = 10 \text{ K}$  and at low energies (Fig. 1(d),  $\hbar\omega = 10 \text{ meV}$ ) the magnetic response starts out as sharply isotropic peaks at the quartet of IC positions schematically illustrated in Fig. 1(a), with essentially no scattering at  $\mathbf{Q} = (\pi, \pi)$  and no evidence for the streaks sketched in Fig. 1(b) and 1(c). The isotropy of the peaks and absence of obvious streaks implies [9, 10] that the magnetic correlations are 2D and immediately rules out any scenario based on a naive subdivision of the material into weakly coupled magnetic stripes. Until now, the extent of this isotropy has not been clear because data have been collected using instruments whose resolution functions are highly anisotropic. If a stripe picture is used to interpret our data, there must be strong inter-stripe as well as intra-stripe exchange coupling.

Warming to just above  $T_c$  (Fig. 1(e)), the IC peaks weaken, as spectral weight is shifted to fill the spin gap at lower energy [7]. We gain dramatic new knowledge by going to  $30 \text{ meV}$  (Fig. 1(f)), where we see that the peaks are no longer well-defined. Instead, the scattering appears more as a “box” surrounding  $(\pi, \pi)$ , and there is now also substantial scattering at  $(\pi, \pi)$ .

In Fig. 2, we examine the data in more detail by looking at constant-energy cuts through the images in Fig. 1. At  $10 \text{ meV}$ , Fig. 2(a) displays the IC peaks at low energies, while in Fig. 2(b) we see very weak sides to the IC “box”. By increasing  $E$  to  $30 \text{ meV}$  it is clear that the response has moved in towards  $(\pi, \pi)$  (Fig. 1), meaning that it is dispersive. In addition, the peaks lose definition – the corners (Fig. 2(c)) are now no sharper than the walls (Fig. 2(d)) of the “box”, and both have broadened so that there is considerable scattering even at  $(\pi, \pi)$ . This transition to broader, continuum like scattering implies that we are not dealing with well-defined bosonic

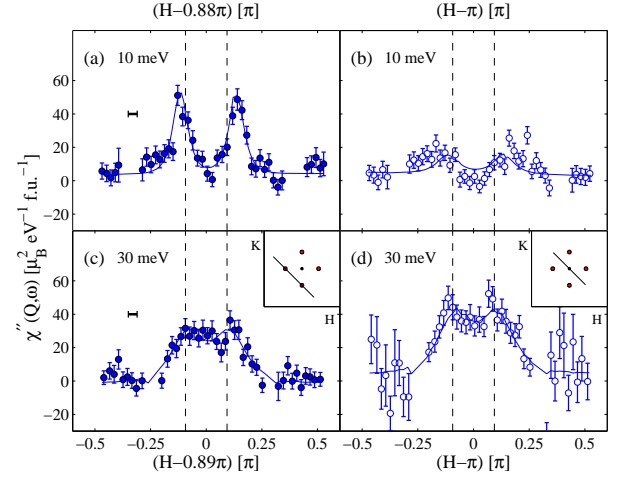


FIG. 2: Constant energy cuts from MAPS through  $\chi''(\mathbf{Q}, \omega)$  for  $\text{La}_{1.84}\text{Sr}_{0.16}\text{CuO}_4$  at  $T = 10 \text{ K}$ . The scan trajectory is transverse as shown in the insets to (c) and (d). (a) and (b):  $\hbar\omega = 10 \text{ meV}$ ; (c) and (d):  $\hbar\omega = 30 \text{ meV}$ . Solid lines: fits to the model discussed in the text. Vertical dashed lines: fitted peak positions at  $30 \text{ meV}$ . Horizontal bars in (a) and (c) represent the instrumental resolution (FWHM). Using the wide reciprocal space coverage of MAPS it was possible to determine accurately the background at positions away from the magnetic scattering. This background has been subtracted from the data shown here.

modes of a quantum spin liquid or AF. A key result of our work, namely that the IC peaks disperse and cannot be due to conventional propagating modes, is thus seen by straightforward display of the data.

We analysed the momentum-dependent images using

$$\chi''(\mathbf{Q}, \omega) = \sum_{\delta} \frac{\chi_{\delta} \kappa^4(\omega)}{(\kappa^2(\omega) + (\mathbf{Q} - \mathbf{Q}_{\delta}(\omega))^2)^2}, \quad (1)$$

where  $\kappa(\omega)$  is an inverse correlation length, and the sum runs over the four IC positions. A good description of the data was obtained by convoluting the above lineshape with the full instrumental resolution function and fitting it to the data (see Fig. 2). From this analysis values were obtained of the incommensurability  $\delta$ , inverse correlation length  $\kappa(\omega)$ , and intensity  $\chi_{\delta}$  of the magnetic fluctuations. The values of  $\delta$  are plotted in Fig. 4(a). It is as apparent from the fits as from the raw data that the peaks in the response move closer to  $\mathbf{Q} = (\pi, \pi)$  and broaden with increasing energy. No change of  $\delta$  is observed on entering the SC state. To emphasize that dispersion of the IC mode is a generic feature of LSCO we also show data taken using MAPS for an underdoped LSCO sample,  $x=0.10$ , where the initial incommensurability is lower, but the velocity is the same. What is even more remarkable is that the velocity associated with dispersion of the non-propagating spin excitations seen here for the metals is the same ( $\sim 1 \text{ eV \AA}$ ) as that for the propagating spin waves in the parent insulator [1]. Figure 4(b)

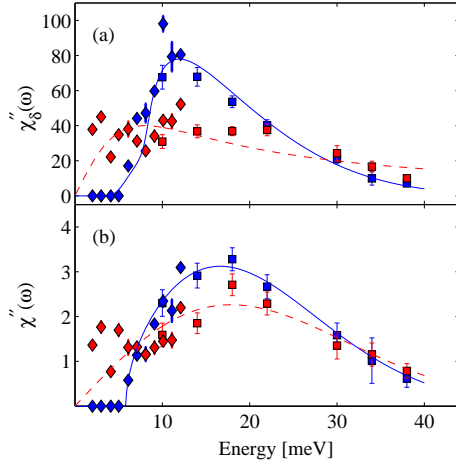


FIG. 3: Energy dependence of  $\chi''(\mathbf{Q}, \omega)$  for optimally doped LSCO in units of  $\mu_B^2 \text{ eV}^{-1} \text{ f.u.}^{-1}$ . (a) Fitted peak amplitude at  $\mathbf{Q}_\delta$ : Superconducting phase, blue symbols; normal phase, red symbols. MAPS data, (squares); triple-axis data (diamonds). (b):  $\chi''(\omega)$  symbols as in (a). Lines are guides to the eye. The region 24-28 meV was found to be strongly contaminated by phonon scattering and was not analysed.

shows the peak width, which above 20 meV is indistinguishable in the normal and SC phases; at lower energies the excitations become more coherent in the SC state[7].

Figure 3(a) displays peak intensities, including data from the same crystals obtained at the RITA spectrometer, Risø, Denmark. As observed previously, superconductivity redistributes the spectral weight from energies below the spin gap  $\Delta = 7 \text{ meV}$ , to higher energies [7]. What is new is that we are able now to see the full extent of the redistribution. The net effect is to produce a peak in  $\chi''(\mathbf{Q}, \omega)$  centred at  $12 \pm 2 \text{ meV}$ , although the redistribution takes place for energies up to about 30 meV. Figure 3(b) presents the local susceptibility  $\chi''(\omega)$  calculated by integrating the response over the 2D Brillouin zone. In the SC phase,  $\chi''(\omega)$  is peaked at  $18 \pm 2 \text{ meV}$ , with a half width at half maximum of  $12 \pm 2 \text{ meV}$ . The normal state mean-squared fluctuating moment [12], calculated from  $\chi''(\omega)$  up to 40 meV is  $\langle m^2 \rangle = 0.062 \pm 0.005 \mu_B^2 (\text{CuO}_2)^{-1}$  and is unchanged on cooling through  $T_c$ . In other words, the spectral weight removed by the opening of the spin gap is preserved and merely shifted to higher energy. A similar shift of spectral weight leads to the formation of a commensurate resonance in lightly doped  $\text{YBa}_2\text{Cu}_3\text{O}_{6+x}$  [12, 13]. In the case of LSCO, the amount of spectral weight shifted is  $\delta \langle m^2 \rangle = 0.010 \pm 0.005 \mu_B^2 (\text{CuO}_2)^{-1}$ , of the same order as  $\delta \langle m^2 \rangle = 0.03 \mu_B^2 (\text{CuO}_2)^{-1}$ , in the resonance of  $\text{YBa}_2\text{Cu}_3\text{O}_{6.6}$  [12]. That the spectral weight in LSCO is conserved already up to 40 meV, makes the existence of the long sought after higher frequency commensurate “resonance” at  $\mathbf{Q} = (\pi, \pi)$  as in YBCO [14, 15, 16] very improbable.

It has often been stated that the IC fluctuations in

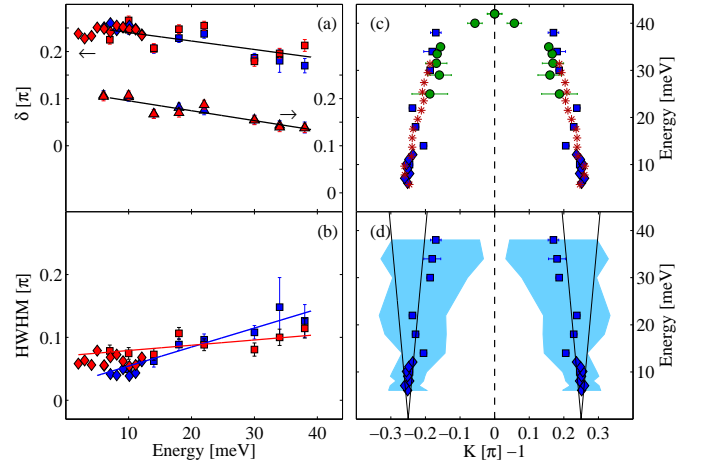


FIG. 4: (a) Incommensurability  $\delta$  in LSCO. Squares: MAPS data for optimal doping,  $x=0.16$ . Triangles: MAPS data for LSCO  $x=0.10$ . Diamonds: triple-axis data on LSCO  $x=0.16$ . Blue symbols, superconducting phase; red symbols, normal state. (b) Energy dependence of the half width at half maximum. Symbols as in (a). (c) Comparison of  $\delta$  for the superconducting phases of optimally doped LSCO (symbols as in (a)) and  $\text{YBCO}_{6.85}$  (circles, [17]), and half the wavevector of the electronic excitations (stars, [4]) observed along the  $(1, 0)$  direction in  $\text{Bi}_2\text{Sr}_2\text{CaCu}_2\text{O}_{8+\delta}$  using STM. (d) Dispersion of the excitations in LSCO. Shaded regions represent the fitted FWHM. Solid lines show the spin-wave velocity of undoped  $\text{La}_2\text{CuO}_4$  with  $J = 156 \text{ meV}$  [1]. The images in (c) and (d) have been symmetrised for display.

LSCO are dispersion-less and a pathology of this single layer material [3, 6]. We argue here that this view is incorrect, even though – at first glance – YBCO, whose fundamental building blocks are  $\text{CuO}_2$ -bilayers, displays a quite different magnetic response. Below  $T_c$ ,  $\chi''(\mathbf{Q}, \omega)$  is dominated by a “resonance” peak at  $\mathbf{Q} = (\pi, \pi)$  ( $E_{\text{res}} = 41 \text{ meV}$  in the case of optimal doping) [14, 15, 16]. Subsequent work revealed that at lower energies,  $E < E_{\text{res}}$ , the response becomes IC [2, 3, 17]. Here we have discovered that the IC response in LSCO is dispersive and remarkably similar to that of  $\text{YBCO}_{6.85}$  as shown in Fig. 4(c). The main difference between the two systems is that the spectral weight redistribution in LSCO takes place well below the energy where the IC modes begin to merge (Fig. 4(d)). In YBCO the larger spin gap results in spectral weight being pushed into the region where the IC modes merge, forming a sharp peak-like response.

While our data resemble those for YBCO, they differ from those for conventional magnets, even with long-period order. For example,  $\text{La}_{1.69}\text{Sr}_{0.31}\text{NiO}_4$  [20], displays two sharply defined modes emanating symmetrically from each IC wavevector as indicated by the solid lines in Fig. 4(d). More recently a study [21] of non-superconducting  $\text{La}_{1.875}\text{Ba}_{0.125}\text{CuO}_4$ , reported asymmetric dispersion but did not specifically address

the lineshape and hence provided no information on any broadening at low energies. In contrast, our high-resolution experiments show that the magnetic excitations disperse in only one direction (inwards), and broaden with increasing energy as rapidly as they disperse (Fig. 4(d)). This means that we are not dealing with propagating spin-wave modes of the type found in conventional magnets.

Instead, our observed response is best described as resulting from a continuum of excitations, indicating that the neutron does not excite the fundamental quasiparticles of the system, but rather coherent pairs, quartets and so on, of quasiparticles. There are several candidates for the underlying quasiparticles. In the ordinary theory of metals the underlying particles are simply electrons and the multi-particle excitations, which neutron scattering would observe are correlated electron-hole pairs. Many theories attempt to explain cuprate spin fluctuations in terms of propagating electrons and holes described by an underlying band structure [22, 23, 24]. However, we lack a single model which describes the remarkable robustness of the velocity with respect to doping (Fig. 4(a)), the absence of measurable dispersion in the spin gap [7], and the universality of the observed response between the bilayer and single layer materials (Fig. 4(c)). A second possibility for the underlying excitations is suggested by returning to the concept of spin-charge separation introduced to the cuprates almost immediately after the discovery of high- $T_c$  [25, 26] superconductivity. Here the fundamental quasiparticles are no longer electrons, carrying spin  $1/2$  and charge  $-e$ ; instead, they are charge neutral objects, spinons carrying spin  $1/2$ , and spin-less objects, holons, carrying charge  $+e$ . While this picture has been verified in 1D [11, 27], its applicability in 2D has been more controversial. Spin-charge separation in the cuprates could occur by sub-division into 1D chains [28], as suggested by the simplest stripe picture [9, 10], or via the effect of competing interactions on 2D quantum systems [29, 30]. Further work is required to differentiate between these two possibilities. Both descriptions imply proximity to quantum critical points, which naturally lead to a magnetic response dominated by non-propagating modes, and has given a very natural framework for understanding the low-frequency properties of an LSCO sample with  $x=0.14$  [31], close to the special filling fraction  $x=1/8$ .

We end by pointing out a correlation between our data and recent STM experiments which have observed dispersing charge quasiparticles. Specifically, the stars in Fig. 4(c) represent the position along  $[1,0]$  of the most obvious IC peak from STM data (positive bias) for “as grown”  $\text{Bi}_2\text{Sr}_2\text{CaCu}_2\text{O}_{8+\delta}$  [4]. Within the conventional band theory of ordinary paramagnetic metals, the loci of the charge and spin responses in  $Q$ - $E$  space should coin-

cide. This is actually not the case – the STM wavevectors when divided by a factor of two line up with the neutron data. This factor of two is of course familiar from the static order seen in conventional magnets [8, 32]. It is quite astonishing that, once this factor of two is included, the spin and electronic response functions measured by neutrons and STM for different materials display nearly identical dispersion. At present the question is open as to whether this correlation between the neutron and STM data sets is coincidental or whether the two are profoundly connected.

We acknowledge stimulating discussions with B. Møller Andersen, S. Davis, S. Chakravarty, T. Giammarchi, P. Hedegård, S. Kivelson, and J. Mesot, and are especially grateful to T. Rosenbaum for his interest and support from the University of Chicago through the National Science Foundation Grant No. DMR-0114798. Work in London was supported by a Wolfson-Royal Society Research Merit Award and the Basic Technology program of the UK research councils.

- 
- [1] S. M. Hayden *et al.*, Phys. Rev. Lett. **67**, 3622 (1991).
  - [2] P. Dai *et al.*, Phys. Rev. B **63**, 054525 (2001).
  - [3] P. Bourges *et al.*, Science **288**, 1234 (2000).
  - [4] J. E. Hoffman *et al.*, Science **297**, 1148 (2002).
  - [5] K. McElroy *et al.*, Nature **422**, 592 (2003).
  - [6] K. Yamada *et al.*, Phys. Rev. B **57**, 6165 (1998).
  - [7] B. Lake *et al.*, Nature **400**, 43 (1999).
  - [8] J. M. Tranquada *et al.*, Nature **375**, 561 (1995).
  - [9] J. Zaanen *et al.*, Philos. Mag. B **81**, 1485 (2001).
  - [10] S. A. Kivelson *et al.*, Rev. Mod. Phys. **75**, 1201 (2003).
  - [11] A. M. Tsvelik, *Quantum field theory in condensed matter physics* (Cambridge University Press, 1996).
  - [12] P. Dai *et al.*, Science **284**, 1344 (1999).
  - [13] C. Stock *et al.*, Phys. Rev. B **69**, 014502 (2004).
  - [14] J. Rossat-Mignod *et al.*, Physica C **185**, 86 (1991).
  - [15] H. F. Fong *et al.*, Phys. Rev. Lett. **78**, 713 (1997).
  - [16] H. A. Mook *et al.*, Nature **395**, 580 (1998).
  - [17] H. M. Rønnow *et al.*, ILL annual report 18 (2000).
  - [18] A. Damascelli *et al.*, Rev. Mod. Phys. **75**, 473 (2003).
  - [19] X. J. Zhou *et al.*, Nature **423**, 398 (2003).
  - [20] P. Bourges *et al.*, Phys. Rev. Lett. **90**, (2003).
  - [21] J. M. Tranquada *et al.*, cond-mat/040162.
  - [22] Y.-J. Kao *et al.*, Phys. Rev. B **61**, 11898 (2000).
  - [23] M. R. Norman, Phys. Rev. B **61**, 14751 (2000).
  - [24] A. V. Chubukov *et al.*, Phys. Rev. B **63**, 180507 (2001).
  - [25] P. W. Anderson, Science **235**, 1196 (1987).
  - [26] D. S. Rokhsar and S. A. Kivelson, Phys. Rev. Lett. **61**, 2376 (1988).
  - [27] D. A. Tennant *et al.*, Phys. Rev. Lett. **70**, 4003 (1993).
  - [28] E. Dagotto and T. M. Rice, Science **271**, 618 (1996).
  - [29] R. Coldea *et al.*, Phys. Rev. B **68**, 134424 (2003).
  - [30] P. A. Lee and N. Nagaosa, Phys. Rev. B **46**, 5621 (1992).
  - [31] G. Aeppli *et al.*, Science **278**, 1432 (1997).
  - [32] O. Zachar *et al.*, Phys. Rev. B **57**, 1422 (1998).